Dispersion Characteristics Analysis of One Dimensional Multiple Periodic Structures and Their Applications to Antennas

Zi Long Ma, Li Jun Jiang, *Senior Member, IEEE*, Shulabh Gupta, *Member, IEEE*, and Wei E.I. Sha, *Member, IEEE*

***Abstract*—This paper proposes a general characterization of one dimensional multiple periodic (MP) structures for electromagnetic transmission and radiation. Studies are conducted from three aspects: Firstly, the dispersion relations of non-dispersive (conventional) and dispersive (composite right/left-handed (CRLH)) materials are analyzed. Regarding each category of materials, detailed analyses for distributed layered media and lumped circuits are presented. Through studies, we found that the periodicity increase opens up multiple stopbands. According to our physical explanations and numerical results, the relation between stopbands and periodicity is clarified. Additionally, the periodicity increase also reduces the separation distance of space harmonic modes along the phase constant axis in the dispersion diagram. Thus, more space harmonic modes are excited in the radiation. This phenomenon results in simultaneous right- and left-handed radiation and multiple radiation beams. Secondly, mathematical formulas for the general dispersion relation and the general Bragg condition of the MP structures are derived. The formulas help to indicate the locations of stopbands and engineer the dispersion relation. Thirdly, applications of the MP structures to phase reversal (PR) antennas are presented. Both transmission and radiation characteristics of the MP structures are validated by the PR antennas experimentally. Single, double and triple periodic structures are comparatively studied.**

***Index Terms*—Dispersion analysis, dispersive structure, leaky-wave antenna, multi-beam radiation, multiple periodic structure, non-dispersive structure, phase reversal antenna.**

I. Introduction

PERIODIC structures have been playing an important role in modern physics and engineering. In the past decades, they have been widely used in optics and microwave areas. For optics, one dimensional periodic structures are often used as gratings, which include stacks of identical parallel planar multi-layer segments. Their transmission characteristics can be analyzed by the matrix theory [1]. Literature studies reveal that if reflected waves from the grating constructively interfere with each other, the transmission stopbands will be opened up. The corresponding condition used to characterize this phenomenon is the famous Bragg condition. In microwave engineering, periodic structures have been applied to studies of antennas [2], [3], especially on the leaky-wave radiation issues [4]–[11].

Metamaterials with their fundamental right/left-hand duality have spurred a significant research interest over the past decade. They were conceptually started by Veselago in 1967 [12] and generally modeled as composite right/left-handed (CRLH) structures [13]–[16]. In practical applications, CRLH structures can be used as the host medium for wave propagation and radiation. Different from the conventional materials, the refractive index of CRLH structure is frequency dependent. Hence, CRLH structures are dispersive.

Recently, a double periodically loaded CRLH structure has been proposed and studied [17]–[20]. In these works, the periodicity of conventional single periodic structure is increased by inserting a different cell between every two adjacent unit cells. Through theoretical studies and practical results, a new right-handed passband was found. However, a general characterization of the multi-periodicity and the systematic analysis for all passbands and stopbands were not mentioned in these works.

In this paper, we provide a general analysis for one dimensional multiple periodic (MP) structures. Different from previous literature works, the general characterization for transmission and radiation performances of both non-dispersive (conventional) and dispersive (CRLH) MP structures are presented. This work aims to explore the general property variation due to the increase of periodicity. From theoretical dispersion relations of the MP layered media (distributed), we found that by increasing the periodicity, extra stopbands will be created. Hence, the original passbands are split into multiple small passbands. This phenomenon happens in both dispersive and non-dispersive cases. Furthermore, we present a more general dispersion relation formula and a general Bragg condition for the MP structures. From another aspect, the MP structures are analyzed by using lumped circuit models. Similar conclusion that the increased periodicity leads to generations of new stopbands is verified theoretically. The relation between the periodicity and the number of stopbands is presented. Additionally, the proposed MP concept is applied to phase reversal (PR) antennas. It is demonstrated that more space harmonic modes are moved into the radiation region in the dispersion diagram. At certain frequency, radiation will be supported by more modes. Hence, si-

Manuscript received April 01, 2014; revised October 21, 2014; accepted October 30, 2014. Date of publication November 03, 2014; date of current version December 31, 2014. This work was supported in part by the HKU Seed Fund 201309160052, US AR120018, NSFC 61271158, and in part by the Hong Kong UGC AoE/PC04/08.

The authors are with the Department of Electrical and Electronic Engineering, The University of Hong Kong, Hong Kong (e-mail: zlma@eee.hku.hk; jianglj@hku.hk).

Color versions of one or more of the figures in this paper are available online at http://ieeexplore.ieee.org.

Digital Object Identifier 10.1109/TAP.2014.2366785

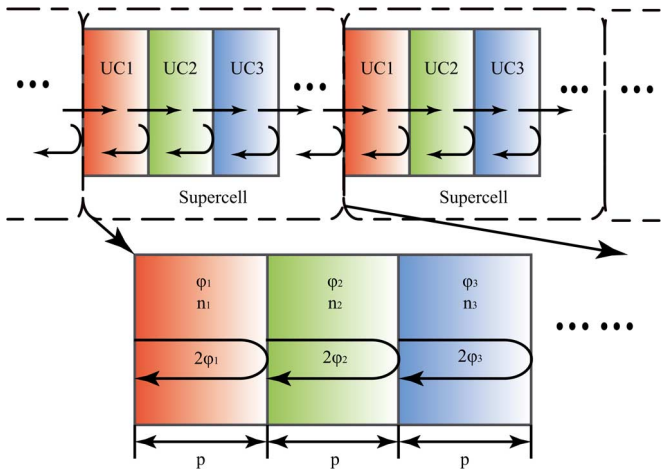

Fig. 1. MP structure illustration. One supercell consists of several different cascaded unit cells, and the supercell periodically repeats in one dimension. Supercells are connected in series. p is the physical length of one unit cell.

multaneous forward and backward radiation and multiple radiation beams become possible. We know that the indoor wireless links have multipath and mutual interference effects that could affect the link quality. One effective solution from the physical layer perspective is to adopt the multi-beam directional antennas. Hence, the MP PR antenna can be a candidate for indoor wireless systems or other multi-beam applications. On the other hand, this work also helps various multi-band component designs. In each analysis, single (SP), double (DP) and triple periodic (TP) structures are presented and compared.

II. Theory

Fig. 1 is a conceptual illustration of the general one dimensional MP structure. The supercell periodically repeats itself along one dimension. Each supercell consists of several different unit cells. All unit cells are connected in series. The physical length of each unit cell is p. A TEM wave is assumed to be incident to the structure from the left side. The time dependence is $e^{+j\omega t}$.

A. Non-Dispersive Media

Firstly, we consider the case when all unit cells are dielectric media. Each unit cell has a different refractive index represented by $n_1, n_2, n_3, \ldots$, and n_m. The boundary interfaces of the kth supercell are denoted by k and $k+1$. The forward (+) and backward (-) propagating waves at these two interfaces are represented by $U_k^{(+)}$, $U_k^{(-)}$, $U_{k+1}^{(+)}$ and $U_{k+1}^{(-)}$. They are related through the transmission matrix,

$$\begin{bmatrix} U_k^{(+)} \\ U_k^{(-)} \end{bmatrix} = \begin{bmatrix} A & B \\ C & D \end{bmatrix} \begin{bmatrix} U_{k+1}^{(+)} \\ U_{k+1}^{(-)} \end{bmatrix} \tag{1}$$

where [A B; C D] is the transmission matrix for one supercell. Based on the matrix theory, it can be written as a product of transmission matrices of unit cells

$$\begin{bmatrix} A & B \\ C & D \end{bmatrix} = \prod_{m=1}^{M} \begin{bmatrix} A_m & B_m \\ C_m & D_m \end{bmatrix} \tag{2}$$

where M is the total number of unit cells in the supercell, and

$$\begin{bmatrix} A_m & B_m \\ C_m & D_m \end{bmatrix} = \frac{1}{2n_{m+1}} \cdot \begin{bmatrix} (n_{m+1}+n_m)e^{-j\varphi_m} & (n_{m+1}-n_m)e^{-j\varphi_m} \\ (n_{m+1}-n_m)e^{j\varphi_m} & (n_{m+1}+n_m)e^{j\varphi_m} \end{bmatrix}. \tag{3}$$

The phase change in one unit cell is $\varphi_m = n_m k_0 p$, where m denotes the unit cell index and k_0 is the free space wave number. According to the Bloch-Floquet theorem, the following condition shall be satisfied

$$\begin{bmatrix} U_{k+1}^{(+)} \\ U_{k+1}^{(-)} \end{bmatrix} = e^{(-j\phi)} \begin{bmatrix} U_k^{(+)} \\ U_k^{(-)} \end{bmatrix} \tag{4}$$

where $\phi = \beta m p$ is the phase change of one supercell. β is the phase constant of the supercell. By substituting (4) into (1), we can obtain the dispersion relation of the supercell,

$$\cos\phi = \frac{A+D}{2}. \tag{5}$$

Using the similar process, we can derive dispersion relations for the DP and TP structures, and write them in the same format.

For the DP structure,

$$\cos\phi = \frac{1}{4n_1n_2} \cdot \left[(n_1+n_2)^2\cos(\varphi_1+\varphi_2) - (n_1-n_2)^2\cos(\varphi_1-\varphi_2)\right]. \tag{6}$$

For the TP structure,

$$\begin{aligned} \cos\phi = \frac{1}{8n_1n_2n_3} & \cdot \left[(n_1-n_2)(-n_2-n_3)(n_1-n_3)\cos(\varphi_1-\varphi_2-\varphi_3)\right. \\ & + (n_1+n_2)(n_2+n_3)(n_1+n_3)\cos(\varphi_1+\varphi_2+\varphi_3) \\ & - (n_1-n_2)(-n_2+n_3)(n_1+n_3)\cos(\varphi_1-\varphi_2+\varphi_3) \\ & \left. - (n_1+n_2)(n_2-n_3)(n_1-n_3)\cos(\varphi_1+\varphi_2-\varphi_3)\right]. \end{aligned} \tag{7}$$

According to the theory of small reflections, due to the existence of discontinuities, multiple wave transmission and reflections happen in the supercell. Physically, the interactions of waves from unit cells contribute to the supercell's dispersion relation. Equations (6), (7) represent these physical interactions in mathematical expressions. If the periodicity is further increased,

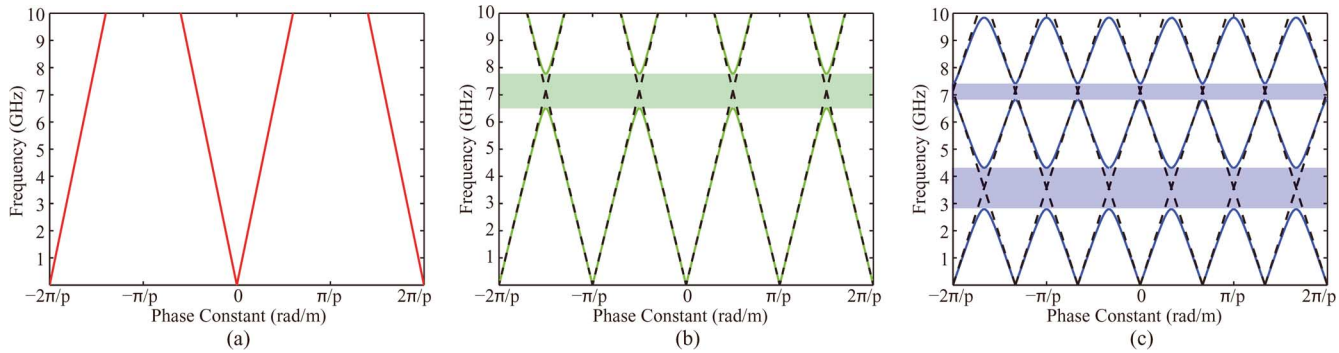

Fig. 2. Theoretical dispersion relations for (a) SP, (b) DP and (c) TP non-dispersive media. $n_1 = 1.5$, $n_2 = 2$, $n_3 = 3.5$, $p = 6$ mm. The solid lines are the dispersion relations. The dash lines stand for the general Bragg condition curves. The shadow regions refer to stopbands.

the physical processes and corresponding mathematical expressions become more complex. The dispersion relation for an arbitrary MP structure can be generally written as (8), shown at the bottom of page. Here

$$\begin{cases} n_{j+1} = n_{j+1-M}, & \text{if } j+1 > M \\ \bar{S}_i^{\,1\times M} = [\pm 1, \pm 1, \pm 1, \ldots, \pm 1] & \\ S_i(j+1) = S_i(j+1-M), & \text{if } j+1 > M \\ \bar{\varphi} = [\varphi_1, \varphi_2, \varphi_3, \ldots, \varphi_M] & \end{cases}. \tag{9}$$

where $\bar{S}_i$ is a sign vector with the dimension of $1 \times M$. It has 2^M permutations. i stands for its ith permutation.

It is well known that for the Bragg grating, in-phase superpositions of reflected waves caused by discontinuities will lead to transmission stopbands. The Bragg condition is often used to indicate the stopbands. Similarly, discontinuities in the MP structures also cause multiple reflections and further result in the occurrence of stopbands. When the reflected waves from unit cells interfere constructively, the reflection will be the strongest and the stopband will appear. As shown in Fig. 1, the round-trip phase of each unit cell is $2\varphi_1, 2\varphi_2, 2\varphi_3, \ldots, 2\varphi_m$. The strongest reflections happen when

$$2\varphi_1 + 2\varphi_2 + 2\varphi_3 + 2\varphi_4 + \ldots + 2\varphi_m = 2\pi q \tag{10}$$

where q is integer. Thus, we can obtain a general Bragg condition for MP structures

$$\sum_{i=1}^{m} \varphi_i = q\pi. \tag{11}$$

For SP, DP and TP structures composed of non-dispersive media, the corresponding dispersion diagrams are computed and shown in Fig. 2. The frequency range is up to 10 GHz. We can see that the SP structure does not have a stopband in the given frequency range while DP and TP structures have one and two stopbands, respectively.

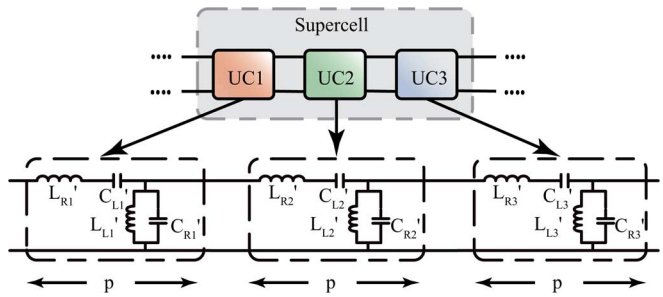

Fig. 3. A three unit cell MP CRLH structure illustration. The equivalent circuit model of one unit cell consists of a series and a shunt LC resonance tanks. L'_R, C'_R, L'_L and C'_L are right/left-handed inductances and capacitances, respectively. They are all per-unit-length components.

Based on the physical process of stopbands induced by discontinuities, we can easily find out the quantified relation between the periodicity M and the maximum number of stopbands N_s for non-dispersive MP structures,

$$N_s = M - 1. \tag{12}$$

It shall be noted that for higher order harmonics along the frequency axis (higher frequency ranges), the conclusion remains the same. Because we keep unit cells' lengths same and $\phi = \beta mp$, the separation distance (along the phase constant axis) of space harmonic modes is reduced accordingly. For SP, DP and TP structures, the separation distances are $2\pi/p$, $2\pi/2p = \pi/p$, $2\pi/3p$, respectively. Fig. 2 also agrees with the general Bragg condition (11). The dash lines are $\sum_{i=1}^{m} \varphi_i/mp$. It is obvious that the frequency points satisfying the general Bragg condition all fall into stopbands. The conventional Bragg condition

$$\cos\phi = \frac{1}{2^{(M+1)}\prod_{i=1}^{M} n_i} \sum_{i=1}^{2^M} \left\{ \left(\prod_{j=1}^{M} S_i(j) \right) \left[\prod_{j=1}^{M} \left(n_j S_i(j) + n_{j+1} S_i(j+1) \right) \right] \cos(\bar{\varphi} \cdot \bar{S}_i) \right\} \tag{8}$$

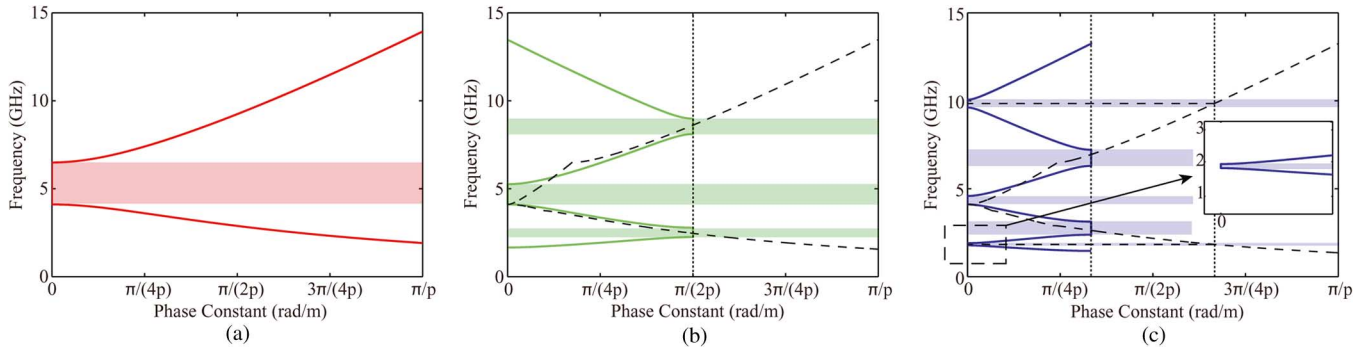

Fig. 4. Theoretical dispersion relations for (a) SP, (b) DP, and (c) TP dispersive media (CRLH) shown in Fig. 3. $L_{R1} = 1.2$ nH, $C_{L1} = 0.5$ pF, $L_{L1} = 1$ nH, $C_{R1} = 1.5$ pF, $L_{R2} = 1.2$ nH, $C_{L2} = 1.5$ pF, $L_{L2} = 1$ nH, $C_{R2} = 1.5$ pF, $L_{R3} = 1.2$ nH, $C_{L3} = 2.5$ pF, $L_{L3} = 1$ nH, $C_{R3} = 1.5$ pF. The solid lines are the dispersion relations. The long dash lines stand for the general Bragg condition curves. The shadow regions refer to stopbands.

for the Bragg grating is determined under two assumptions [1]: (1) unit cells are weakly reflective, and the incident wave is not depleted as it propagates. (2) The secondary reflections are negligible. Hence, the general Bragg condition helps to indicate the locations of stopbands. But the condition points are not exactly at the centers of stopbands.

B. Dispersive Media

For the dispersive material, the CRLH structure is employed as an example. Fig. 3 gives an illustration to the MP CRLH structure and the equivalent circuit model. $L'_{R/L}$ and $C'_{R/L}$ are per-unit-length right/left-handed inductances and capacitances, respectively. The effective refractive index of the CRLH structure can be represented by [16],

$$n(\omega) = c\left(\frac{1}{\omega'_R} - \frac{\omega'_L}{\omega^2}\right) \tag{13}$$

where

$$\omega'_L = \frac{1}{\sqrt{L'_L C'_L}}, \quad \omega'_R = \frac{1}{\sqrt{L'_R C'_R}}. \tag{14}$$

Here c is the light speed.

Substituting (13) into (8), the dispersion relation for CRLH media can be obtained. Fig. 4 presents dispersion relations for SP, DP and TP CRLH structures. To make the theory more general, we start with an unbalanced SP CRLH structure [16]. There is one stopband in its dispersion relation. DP and TP CRLH structures have three and five stopbands, respectively. The relation between the periodicity M and the maximum number of stopbands N_s can be summarized as

$$N_s = 2M - 1. \tag{15}$$

Similar to non-dispersive media, the separation distance of space harmonic modes is also reduced accordingly. For SP, DP and TP CRLH structures, the distances are $2\pi/p$, π/p, $2\pi/3p$, respectively. The general Bragg condition is also verified through this figure. The long dash lines are $\sum_{i=1}^{m} \varphi_i/mp$. This figure shows that the general Bragg condition is also suitable for dispersive materials.

C. Non-Dispersive Lumped Circuits

Next, the dispersion relations of MP lumped circuits are analyzed. The conventional transmission line (TL) model is used for non-dispersive case's analyses. Similar to the layered media, the voltages and currents of the kth lumped circuit supercell can be formulated as

$$\begin{bmatrix} V_k \\ I_k \end{bmatrix} = \begin{bmatrix} A & B \\ C & D \end{bmatrix} \begin{bmatrix} V_{k+1} \\ I_{k+1} \end{bmatrix}. \tag{16}$$

Based on the Bloch-Floquet theorem, we have

$$\begin{aligned} V_{k+1} &= V_k e^{-\gamma mp} \\ I_{k+1} &= I_k e^{-\gamma mp}. \end{aligned} \tag{17}$$

Substituting (17) into (16), we obtain

$$\cos(\gamma mp) = \frac{A+D}{2}. \tag{18}$$

Here γ is the propagation constant and $\gamma = \alpha + j\beta$. Note that [A B; C D] is the transmission matrix with respect to the supercell. It also can be defined by the product of unit cells' transmission matrices as (2).

According to the transmission line theory, elements of unit cells' transmission matrices can be represented as [2]

$$\begin{aligned} A_m &= \cos\beta l_m \\ B_m &= jZ_{0m}\sin\beta l_m \\ C_m &= jY_{0m}\sin\beta l_m \\ D_m &= \cos\beta l_m \end{aligned} \tag{19}$$

where Z_{0m} and l_m are the characteristic impedance and the physical length of the mth unit cell, respectively. The physical lengths of unit cells are identical, $l_m = p$. Substituting (19) into (2) and following the same derivations in Section II-A, the dispersion relations can be obtained.

Fig. 5 shows dispersion relations of SP, DP and TP TLs. The results are consistent with previous analyses. Due to the multi-periodicity, DP and TP cases have new stopbands. The frequency range from 0 GHz to 8 GHz covers two harmonic

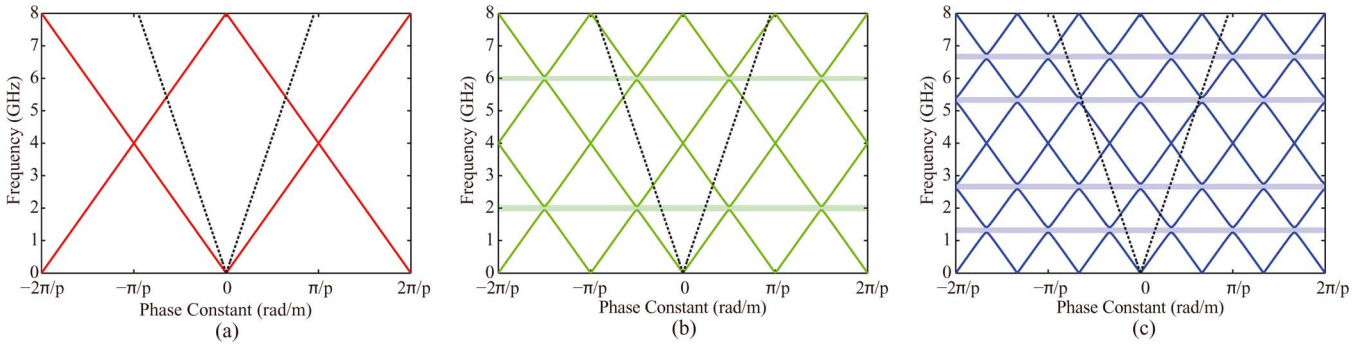

Fig. 5. Theoretical dispersion relations for (a) SP, (b) DP, and (c) TP non-dispersive lumped circuits (strip line TLs). $Z_{01} = 100$ ohm, $Z_{02} = 110$ ohm, $Z_{03} = 130$ ohm, physical length of unit cell $p = \lambda_g/2$ which is at 4 GHz. The solid lines are the dispersion relations. The dash lines are the wave vectors in the free space (air lines). The shadow regions refer to stopbands.

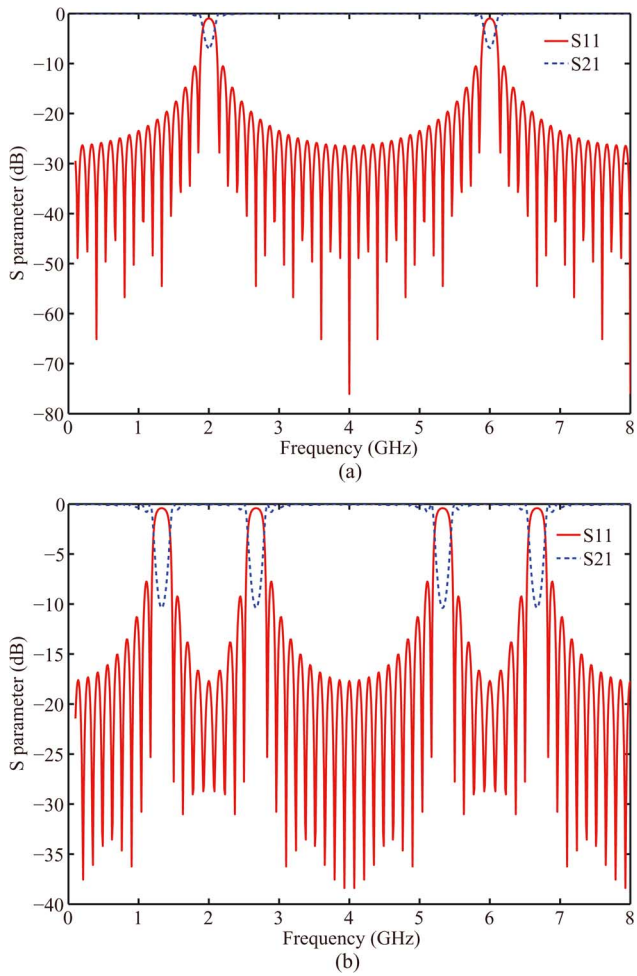

Fig. 6. Simulated S-parameters for (a) DP and (b) TP strip line TLs. $Z_{01} = 100$ ohm, $Z_{02} = 110$ ohm, $Z_{03} = 130$ ohm, physical length of unit cell $p = \lambda_g/2$ which is at 4 GHz.

frequencies. Hence, there are two and four stopbands for DP and TP cases, respectively. Within the frequency range from 0 GHz to 4 GHz, the number of stopbands also obeys the relation (12). In addition, different from layered media, we take the radiation issues into the consideration for the lumped circuits. In Fig. 5, due to the reduction of the space harmonic separation,

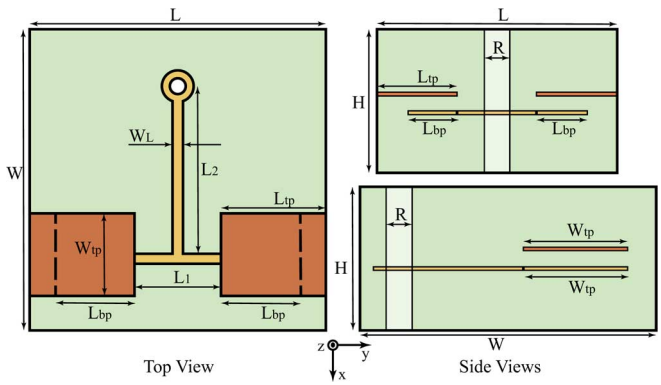

Fig. 7. Configuration of MIM structure. The physical dimensions are $L = 37.048$ mm, $W = 50$ mm, $H = 3.302$ mm, $W_{tp} = 12.7$ mm, $L_{tp} = 14.024$ mm, $L_{bp} = 12.5$ mm, $L_1 = 9$ mm, $L_2 = 23.016$ mm, $W_L = 1.016$ mm and $R = 2.048$ mm.

more modes are shifted to leaky-wave regions. For example, the DP structure simultaneously has one right-handed (parallel phase and group velocity) mode and one left-handed (antiparallel phase and group velocity) radiation mode in the leaky-wave region at 6.5 GHz. Since these two modes have different phase constants, based on the leaky-wave theory, two separated radiation beams will be generated. Similarly, for the TP structure, it has more right/left-handed radiation modes at a specified frequency. Hence, MP structures can realize the multi-beam radiation.

To further examine the stopbands' properties, the MP TLs are simulated in commercial software Agilent Advanced Design System (ADS). Fig. 6 shows the S-parameter results. In DP and TP cases, the stopbands appear at {2, 6} GHz and {1.3, 2.6, 5.3, 6.7} GHz, respectively. The results in Fig. 5 and Fig. 6 show very good agreement for the stopband prediction.

D. Dispersive Lumped Circuits

The transmission matrix of CRLH lumped circuit is [16]

$$\begin{bmatrix} A_m & B_m \\ C_m & D_m \end{bmatrix} = \begin{bmatrix} 1 & Z_m/2 \\ 0 & 1 \end{bmatrix} \begin{bmatrix} 1 & 0 \\ Y_m & 1 \end{bmatrix} \begin{bmatrix} 1 & Z_m/2 \\ 0 & 1 \end{bmatrix} = \begin{bmatrix} 1 + Z_m Y_m/2 & Z_m(1 + Z_m Y_m/4) \\ Y_m & 1 + Z_m Y_m/2 \end{bmatrix} \quad (20)$$

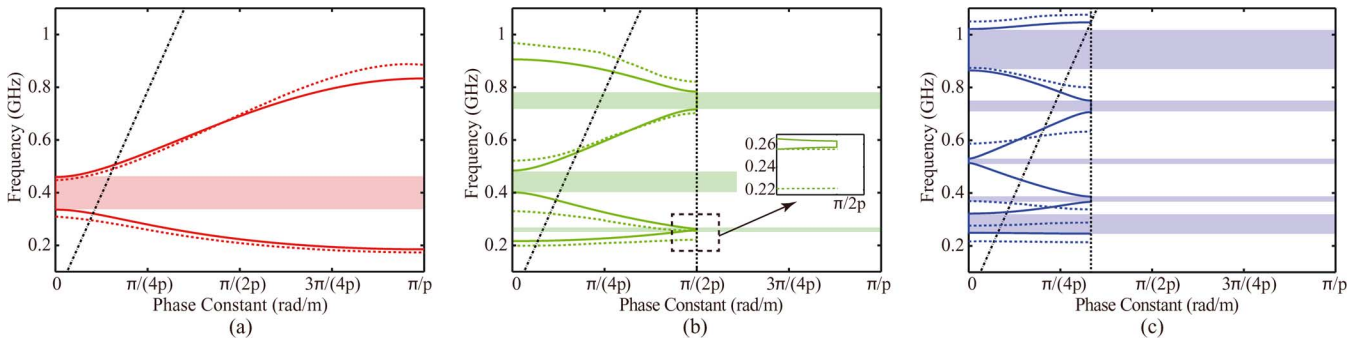

Fig. 8. Simulated and theoretical dispersion relations for (a) SP, (b) DP, and (c) TP dispersive lumped circuits (MIM CRLH TLs). The colored solid and dash lines are theoretical and simulated results, respectively. The long-short dash lines are wave vectors in free space (air lines). The shadow regions refer to the stopbands.

where

$$Z_m = j\left(\omega L_{Rm} - \frac{1}{\omega C_{Lm}}\right)$$
$$Y_m = j\left(\omega C_{Rm} - \frac{1}{\omega L_{Lm}}\right). \quad (21)$$

Here L_{Rm}, L_{Lm}, C_{Rm}, and C_{Lm} are lumped inductances and capacitances, respectively. The equivalent circuit model is same with that of Fig. 3. By substituting (20) into (2) and following the same derivations in Section II-A, the dispersion relations can be computed. To examine the theory, metal-insulation-metal (MIM) CRLH structures are simulated in the full wave simulation software HFSS. Fig. 7 shows the simulated configurations. In order to obtain different unit cells, the parameter L_{bp} is changed to $L_{bp}/2$ and $L_{bp}/4$ for DP and TP cases, respectively. The corresponding LC values are extracted to be $L_{Rm} \in \{25, 24, 23.5\}$ nH, $L_{Lm} \in \{12, 12, 12\}$ nH, $C_{Rm} \in \{10, 8, 6\}$ pF, and $C_{Lm} \in \{9, 5, 2\}$ pF. The dispersion relations for SP, DP, and TP MIM CRLH structures are simulated through the eigenmode analysis solver. The results are compared with theoretical calculations as shown in Fig. 8. The results demonstrate good agreement. Hence, similar conclusions for dispersive lumped circuits can be obtained: due to the multi-periodicity, the separation interval of space harmonics is reduced and new stopbands are created. However, in our implementation, the realizations of impedance matchings of MP CRLH TLs are very challenging.

III. Multiple Periodic Phase Reversal Antenna

In this part, an MP PR antenna is proposed. DP and TP PR antennas are demonstrated. The conventional (single periodic) PR antenna is also shown for comparison.

A. Antenna Configurations and Operating Principles

The PR antenna is a periodically loaded antenna [21]–[23]. It supports leaky-wave radiation and can realize the angular scanning through the frequency sweep. The basic unit cell of PR antenna is an offset parallel strip line (OPS) with the differential current and a crossover section. In this paper, a symmetric PR unit cell is used as shown in Fig. 9. The figure illustrates a top view of the proposed unit cell. The red and blue regions are top and bottom metal layers, respectively. The

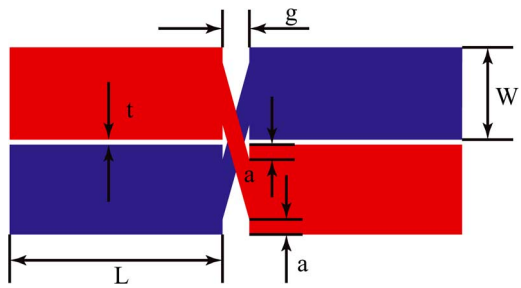

Fig. 9. Unit cell configuration of MP phase reversal antenna.

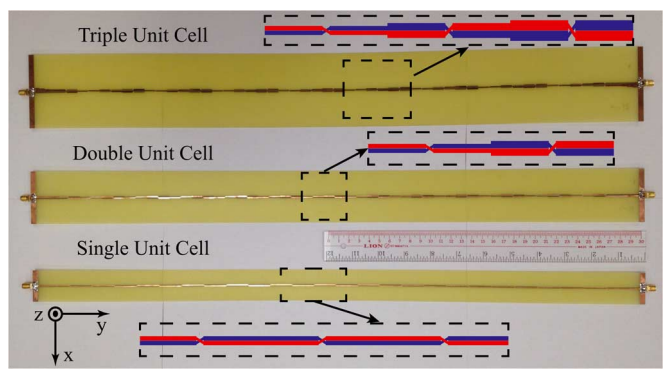

Fig. 10. Prototypes of SP, DP and TP phase reversal antennas.

TABLE I
Antenna Parameters

	L (mil)	W (mil)	t (mil)	g (mil)	a (mil)	Z_0 (ohm)
1st Unit Cell	400	30	2	50	5	130
2nd Unit Cell	400	50	2	50	10	110
3rd Unit Cell	400	70	2	50	17	100

crossover section is in the center of the unit cell. Two OPS lines are symmetrically placed on the left and right sides of the crossover, respectively. To realize the MP configuration, different unit cells are introduced by changing characteristic impedances. Fig. 10 shows the prototypes of SP, DP and TP PR antennas. Their physical dimensions are listed in Table I. The dimension W is changed from 30 to 70 mil (step is 20 mil) for SP, DP and TP cases. Correspondingly, the parameter a is changed to obtain the good impedance matching. The three-stage balun and impedance-transformer transition in [21]

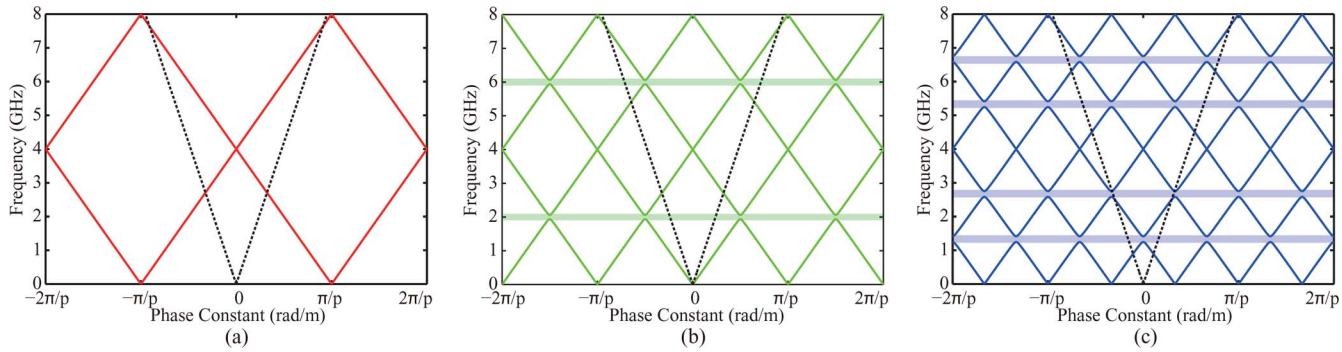

Fig. 11. Theoretical dispersion relations for (a) SP, (b) DP, and (c) TP phase reversal antennas. The solid lines are the dispersion relations. The dash lines are the wave vectors in the free space (air lines). The shadow regions refer to stopbands.

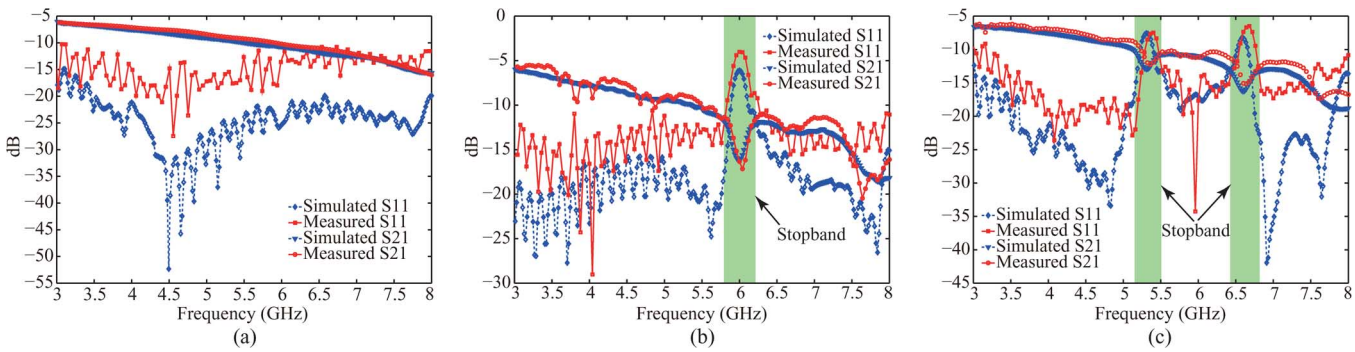

Fig. 12. Simulated and measured S-parameters of (a) SP, (b) DP, and (c) TP phase reversal antennas shown in Fig. 10. The shadow regions refer to stopbands.

are adopted in this design. The substrate is 0.8 mm thick FR4 with the dielectric constant 4.4 and loss tangent 0.02. The characteristic impedances of unit cells are also listed in Table I.

The PR antenna is a TEM type TL. Each unit cell has excellent transmission property. The dispersion relation of conventional PR antenna can be characterized based on the TL model. However, because of the phase reversal phenomenon induced in each unit cell, an extra phase shift π is generated for each unit cell [23]–[25]. Due to different periodicities, the phase shifts are π, 2π and 3π for SP, DP and TP supercells, respectively. By using the method shown in Section II-C, the dispersion relations of SP, DP and TP PR antennas are given in Fig. 11. This figure verifies conclusions same to those of Part II. For DP and TP, two frequency intervals are covered by stopbands from 0 GHz to 8 GHz. In each interval (4 GHz), they have one and two stopbands, respectively. The stopbands appear at $\{2, 6\}$ GHz and $\{1.3, 2.6, 5.3, 6.7\}$ GHz, respectively. The separations of space harmonics are reduced accordingly. More radiation modes supporting simultaneous right- and left-handed radiation appear at higher frequencies.

B. Simulations and Experiments

The antennas are designed to cover from 3 GHz to 8 GHz. 24 unit cells are used for each antenna. Fig. 12 presents the simulated and measured S-parameters of SP, DP and TP PR antennas. The measured results show very good agreement with the simulation. From the measured data, the SP PR is matched below -10 dB over the entire frequency range, and there is no stopband. The DP PR has one stopband at 6.04 GHz. The corresponding S11 and S21 magnitudes are -4.058 dB and -17.16 dB, respectively. The stopband width is almost 0.5 GHz. The TP PR has two stopbands at 5.4 GHz and 6.68 GHz. Their S11 and S21 magnitudes are $\{-7.487, -12.27\}$ dB and $\{-6.495, -14.78\}$ dB, respectively. The stopband widths are all around 0.3 GHz.

Fig. 13 shows the normalized simulated and measured radiation patterns of three antennas in the y-z plane. Five radiation patterns are presented for each antenna. It is obvious that the DP PR at $\{6.5, 7.2\}$ GHz and the TP PR at $\{5, 5.7\}$ GHz have two radiation modes simultaneously. At these frequencies, both right- and left-handed radiation are excited. At 7.2 GHz, the TP PR has three radiation modes. Hence, three beams are generated in each half plane. These radiation patterns show very good agreement with dispersion relations in Fig. 11. In Fig. 14, the measured and simulated gains of the proposed SP, DP and TP PR antennas are presented. Obvious gain drops can be found at the stopbands' frequencies: 6.04 GHz for DP PR and $\{5.4, 6.68\}$ GHz for TP PR.

IV. Conclusion

The dispersion relations of the general MP structure are analyzed theoretically for layered media and lumped circuits. Both non-dispersive (conventional) and dispersive (CRLH) materials are discussed. A general dispersion relation and a general Bragg condition are presented. They can be used to locate the positions of stopbands and engineer the dispersion property. When the periodicity increases, multiple stopbands are created due to more reflections from unit cells. MP structures can reduce the separation distances of space harmonic modes. More radiation modes

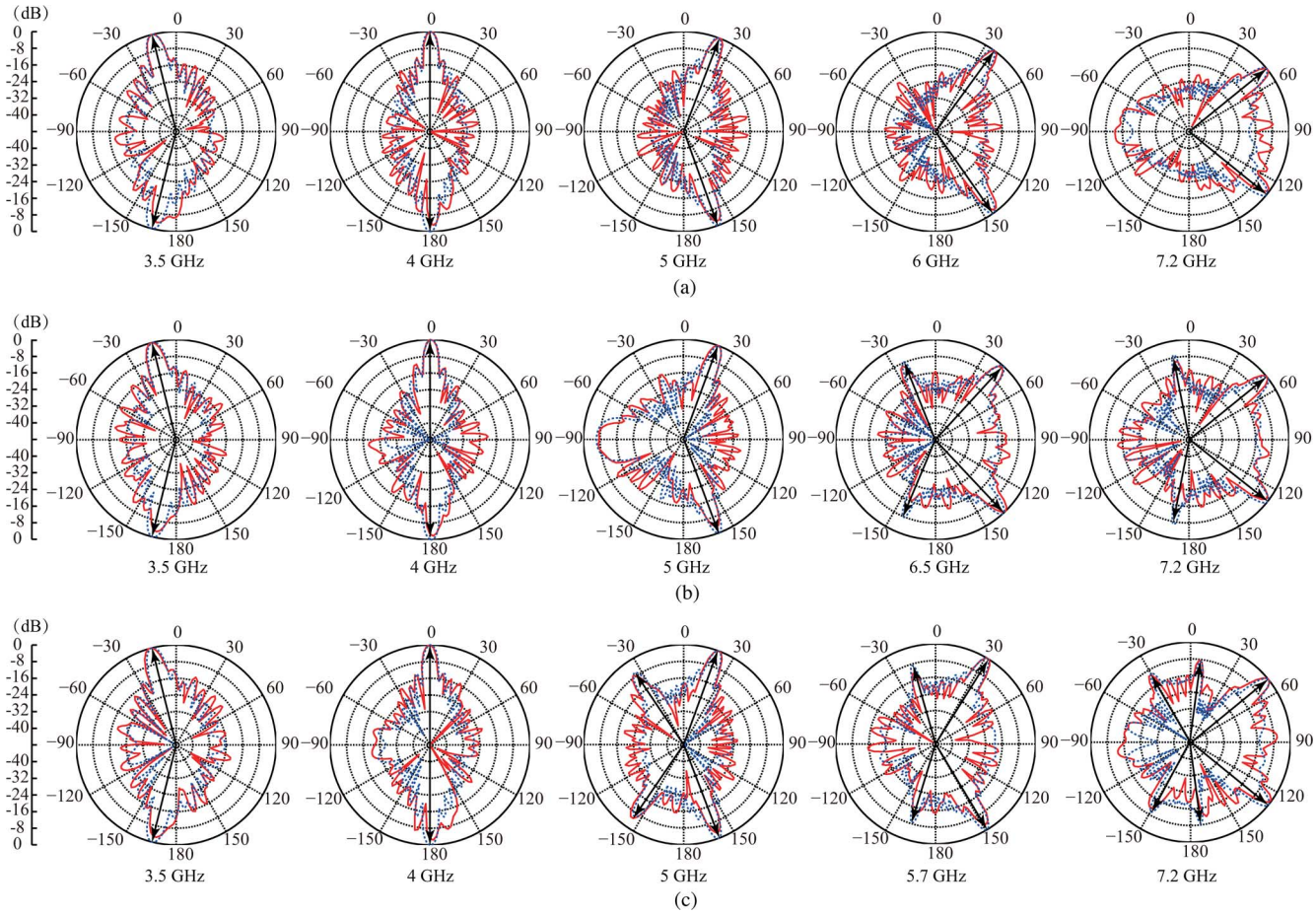

Fig. 13. Simulated and measured radiation patterns E_ϕ in y-z plane for (a) SP, (b) DP, and (c) TP phase reversal antennas at {3.5, 4, 5, 6, 7.2} GHz {3.5, 4, 5, 6.5, 7.2} GHz and {3.5, 4, 5, 5.7, 7.2} GHz, respectively. The red solid lines and the blue dash lines are measured and simulated results, respectively.

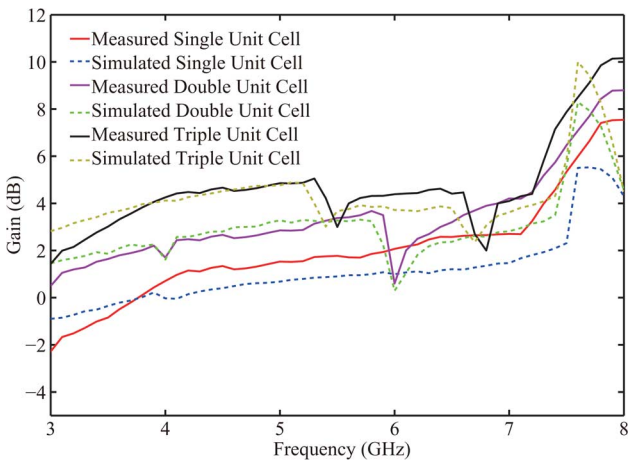

Fig. 14. Measured and simulated antenna gains of the proposed SP, DP, and TP phase reversal antennas.

are excited to simultaneously support right- and left-handed radiation and multi-beam. The applications of MP structure to PR antennas are presented. Their transmission and radiation properties are experimentally demonstrated and compared with the proposed theory.

ACKNOWLEDGMENT

The authors would like to acknowledge the help from State Key Laboratory of Millimeter Waves, City University of Hong Kong.

REFERENCES

[1] B. E. A. Saleh and M. C. Teich, *Fundamentals of Photonics*, 2nd ed. New York, NY, USA: Wiley, 2007.
[2] D. M. Pozar, *Microwave Engineering*, 3rd ed. New York, NY, USA: Wiley, 2004.
[3] C. A. Balanis, *Antenna Theory: Analysis and Design*, 2nd ed. New York, NY, USA: Wiley, 1996.
[4] P. Burghignoli, G. Lovat, and D. R. Jackson, "Analysis and optimization of leaky-wave radiation at broadside from a class of 1D periodic structures," *IEEE Trans. Antennas Propag.*, vol. 54, pp. 2593–2604, Sep. 2006.
[5] D. Deslandes and K. Wu, "Accurate modeling, wave mechanisms, design considerations of a substrate integrated waveguide," *IEEE Trans. Microw. Theory Tech.*, vol. 54, no. 6, pp. 2516–2526, Jun. 2006.
[6] F. Xu, K. Wu, and X. Zhang, "Periodic leaky-wave antenna for millimeter wave applications based on substrate integrated waveguide," *IEEE Trans. Antennas Propag.*, vol. 58, no. 2, pp. 340–347, Feb. 2010.
[7] E. M. OConnor, D. R. Jackson, and S. A. Long, "Extension of the Hansen-Woodyard condition for endfire leaky-wave antennas," *IEEE Antennas Wireless Propag. Lett.*, vol. 9, pp. 1202–1204, 2010.
[8] A. Ishimaru, *Electromagnetic Wave Propagation, Radiation, Scattering*. Englewood Cliffs, NJ, USA: Prentice-Hall, 1991.
[9] A. A. Oliner and D. R. Jackson, "Leaky-wave antennas," in *Antenna Engineering Handbook*, J. Volakis, Ed., 4th ed. New York, NY, USA: McGraw-Hill, 2007, ch. 10.
[10] C. Caloz, T. Itoh, and A. Rennings, "CRLH metamaterial leaky-wave and resonant antennas," *IEEE Trans. Antennas Propag. Mag.*, vol. 50, no. 5, pp. 25–49, Oct. 2007.
[11] S. Lin, C. Caloz, and T. Itoh, "Metamaterial-based electronically controlled transmission line structure as a novel leaky-wave antenna with tunable angle and beamwidth," *IEEE Trans. Microw. Theory Tech.*, vol. 53, no. 1, pp. 161–173, Jan. 2005.
[12] V. G. Veselago, "The electrodynamics of substances with simultaneously negative values of ϵ and μ," *Sov. Phys.-Usp.*, vol. 10, no. 4, pp. 509–514, Jan.–Feb. 1968.

[13] A. Lai, C. Caloz, and T. Itoh, "Composite right/left-handed transmission line metamaterials," *IEEE Microw. Mag.*, vol. 5, no. 3, pp. 34–50, Sep. 2004.
[14] A. Sanada, C. Caloz, and T. Itoh, "Characteristics of the composite right/left-handed transmission lines," *IEEE Microw. Wireless Compon. Lett.*, vol. 14, no. 2, pp. 68–70, Feb. 2004.
[15] L. Liu, C. Caloz, and T. Itoh, "Dominant mode leaky-wave antenna with backfire-to-endfire scanning capability," *Electron. Lett.*, vol. 38, no. 23, pp. 1414–1416, Nov. 2002.
[16] C. Caloz and T. Itoh, *Electromagnetic Metamaterials: Transmission Line Theory and Microwave Applications*. New York, NY, USA: Wiley, 2006.
[17] J. Cheng, A. Arokiaswami, and M. Tsutsumi, "Leaky-wave characteristics from double periodic composite right-/left-handed transmission lines," *IET Microw. Antennas Propag.*, vol. 5, no. 12, pp. 1399–1407, Jul. 2011.
[18] J. Cheng and A. Arokiaswami, "Double periodic composite right/left handed substrate integrated waveguide," in *Proc. Asia-Pacific Microw. Conf.*, 2011, pp. 429–432.
[19] J. Cheng and A. Arokiaswami, "Leaky-wave radiation behavior from a double periodic composite right/left-handed substrate integrated waveguide," *IEEE Trans. Antennas Propag.*, vol. 60, no. 4, pp. 1727–1735, Apr. 2012.
[20] J. Cheng and A. Arokiaswami, "Double periodic composite right/left handed transmission line and its applications to compact leaky-wave antennas," *IEEE Trans. Antennas Propag.*, vol. 59, no. 10, pp. 3679–3686, Oct. 2011.
[21] N. Yang, C. Caloz, and K. Wu, "Full-space scanning periodic phase-reversal leaky-wave antenna," *IEEE Trans. Antennas Propag.*, vol. 58, no. 10, pp. 2619–2632, Oct. 2010.
[22] N. Yang, C. Caloz, and K. Wu, "Wideband phase-reversal antenna using a novel banswidth enhancement technique," *IEEE Trans. Antennas Propag.*, vol. 58, no. 9, pp. 2823–2830, Sep. 2010.
[23] N. Yang, C. Caloz, and K. Wu, "Fixed beam frequency-tunable phase-reversal coplanar stripline antenna array," *IEEE Trans. Antennas Propag.*, vol. 57, no. 3, pp. 671–681, Mar. 2009.
[24] A. Hessel, *Antenna Theory, Part II*, R. E. Collin and R. F. Zucker, Eds. New York: McGraw-Hill, 1969, ch. 19.
[25] C. S. Franklin, "Improvements in wireless telegraph and telephone aerials," British patent 242.342, Aug. 5, 1924.

Zi Long Ma received the B.S. degree from South China University of Technology, Guangzhou, in 2010 and the M.S. degree from The University of Hong Kong, Hong Kong, in 2011, all in electronic engineering. He is currently working toward the Ph.D. degree at the Department of Electrical and Electronic Engineering, The University of Hong Kong, Hong Kong.

His research interests include periodic structures, leaky-wave antennas, composite right/left handed structures and RFID antennas.

Li Jun Jiang (S'01–M'04–SM'13) received the B.S. degree in electrical engineering from the Beijing University of Aeronautics and Astronautics, Beijing, China, in 1993, the M.S. degree from the Tsinghua University, China, in 1996, and the Ph.D. degree from the University of Illinois at Urbana-Champaign, Champaign, IL, USA, in 2004.

From 1996 to 1999, he was an application Engineer with Hewlett-Packard. Since 2004, he has been a Postdoctoral Researcher, a research staff member, and a Senior Engineer at the IBM T.J. Watson Research Center. Since the end of 2009, he is an Associate Professor with the Department of Electrical and Electronic Engineering, University of Hong Kong. His research interests focus on electromagnetics, computational electromagnetics, IC signal/power integrity, IC EMC/EMI, antennas, multidisciplinary EDA solutions, RF and microwave technologies, high performance computing (HPC), etc.

Prof. Jiang is a member of the IEEE AP-S and IEEE MTT-S, ACES, and the Chinese Computational Electromagnetics Society. He received the HP STAR Award in 1998. In 2003, he received the IEEE MTT Graduate Fellowship Award, and in 2004, the Y.T. Lo Outstanding Research Award. In 2008, he received the IBM Research Technical Achievement Award. He is an Editor of *Progress In Electromagnetics Research*, an Associate Guest Editor of a Special Issue of the IEEE PROCEEDINGS in 2011 2012, and a Guest Editor of the *Journal of Electrical and Computer Engineering* Special Issue in 2013. He was the Semiconductor Research Cooperation (SRC) Industrial Liaison for several academic projects. He was the SRC packaging High Frequency Tel-Topic chair. He was a TPC member of IEEE Electrical Design for Advanced Packaging and Systems (EDAPS) since 2010, a TPC member of 2013 IEEE International Conference on Microwave Technology & Computational Electromagnetics (ICMTCE), a scientific committee member of 2010 Workshop on Simulation and Modeling of Emerging Electronics (SMEE), a special session organizer of IEEE EDAPS, the International Review of Progress in Applied Computational Electromagnetics (ACES), Asia-Pacific Radio Science Conference (AP-RASC), a co-organizer of HKU Computational Science and Engineering Workshops in 2010–2012, a TC-9 and TC-10 member of IEEE EMC-S since 2011, the TPC Chair of the 7th International Conference on Nanophotonics (ICNP), the TPC member of the 3rd Conference on Advances in Optoelectronics and Micro/Nano Optics (AOM), a Co-Chair of International Workshop on Pulsed Electromagnetic Field, Delft, The Netherlands, 2013, Chair of the 14th IEEE Hong Kong AP/MTT Postgraduate Conference, and session chair of many international conferences. He also serves as a Reviewer of the IEEE TRANSACTIONS on several topics, and other primary electromagnetics and microwave related journals.

Shulabh Gupta (A'06–M'11) was born on December 14, 1982, in India. He received B.Tech. degree in electronic engineering from the Indian School of Mines, Dhanbad, India, in 2004, the M.S. degree in telecommunications from the Institut National de la Recherche Scientifique Énergie Matériaux Télécommunications Research Center (INRS-EMT), Université du Quebec, Montreal, QC, Canada, in 2006, and the Ph.D. degree in electrical engineering from the École Polytechnique of Montréal, Montreal, QC, Canada, in 2012. His M.S. thesis research concerned optical signal processing related to the propagation of light in linear and nonlinear optical fibers and fiber Bragg gratings. His Ph.D. research concerned the analog signal-processing techniques using dispersion engineered structures.

From December 2009 to May 2010, he was a Visiting Research Fellow with the Tokyo Institute of Technology, Tokyo, Japan, where he was involved with the application of high impedance surfaces for oversized slotted waveguide antennas. In 2012, he was a Postdoctoral Fellow at the University of Colorado at Boulder, Boulder, CO, USA, where he worked on the design and characterization of high-power UWB antennas. From 2012 to 2014, he was with the University of Hong Kong as a Postdoctoral Fellow where he engaged in research concerned with multi-functional travelling-wave leaky-wave antennas for RFID and imaging applications. Currently he is a Postdoctoral Fellow in the Electrical Engineering Department, École Polytechnique of Montreal, Montreal, QC, Canada.

Dr. Gupta was a recipient of the Young Scientist Award of EMTS Ottawa 2007, URSI-GA, Chicago 2008, and ISAP Jeju 2011. His thesis won the Best Doctoral Dissertation Award at the École Polytechnique of Montreal, Montreal, Prix d'excellence de l'Association des doyens desétudes supérieures au Quebec (ADESAQ) Edition 2013 in Quebec, and the Academic Gold Medal of the Governor General of Canada.

Wei E.I. Sha (M'08) received the B.S. and Ph.D. degrees in electronic engineering from Anhui University, Hefei, China, in 2003 and 2008, respectively.

From July 2008 to May 2012, he was a Postdoctoral Research Fellow with the Department of Electrical and Electronic Engineering, University of Hong Kong, where he is now a Research Assistant Professor. He has published over 50 peer-reviewed journal papers, contributed to three book chapters and coauthored a book on wavelet theory and applications. He has broad research interests in applied and computational electromagnetics, nano-optics and quantum-optics, solar cells and optoelectronics, multiphysics modeling and understanding, etc.

Dr. Sha is a member of the IEEE Photonics Society and IEEE Antennas and Propagation Society. He is also a member of OSA. He has been serving as a reviewers for IEEE, OSA, AIP, APS and Nature Publishing Group journals.